Turbulent Poiseuille flow modelling by an enhanced Prandtl-Driest mixing length

Bo-Hua Sun[1]

[1]School of Civil Engineering & Institute of Mechanics and Technology
Xi'an University of Architecture and Technology, Xi'an 710055, China
email: sunbohua@xauat.edu.cn

(Dated: Jan. 15, 2022)

The turbulent Poiseuille flow between two parallel plates is one of the simplest possible physical situation, which has been studied intensively in literature. Different mixing lengths are used, however no one has simultaneously considered boundary conditions of two walls together with damping effects from two walls. In this paper, we propose an enhanced Prandtl-Driest mixing length that not only satisfies all boundary conditions but including both walls' damping effects. With our new formulations, we numerically solve the problem and even further propose an explicit approximate solutions. As applications of our solutions, the total velocity, the total shear stress, the energy dissipation density, the energy balance, the Kolmogorov scale law and friction of turbulent Poiseuille flow are to be studied in detail. The study discoveries that the high heels profiles of both mean and total velocity are universal for all wall-bounded turbulent flows.

Keywords: Turbulent flow, Poiseuille flow, Prandtl mixing length, high heels velocity profile, Reynolds number

I. INTRODUCTION

The theory of the turbulence boundary layer dates back to 100 years ago. In 1921, Prandtl discovered that almost all boundary-layer movements in nature are turbulent rather than laminar [1–12]. The understanding of fully developed turbulence remains a major unsolved problem of physics. A challenge there is how to use what we understand of this problem to build-up a closure method, that is to express the time averaged turbulent stress tensor as a function of the time averaged velocity field [1–3, 13–31]. For the modeling of mean velocity profiles, notable works include [16, 17], all building on the multi-layer concept of turbulent wall flows. For the Reynolds stresses (including Reynolds shear stress and normal stresses), [18] develop a similar multilayer model for channels and pipes by using the symmetry argument. Recently, on the Reynolds number scaling of near wall fluctuations, [19] and [20] propose the 'law of bounded dissipation' and show that near wall peaks of turbulent dissipations, pressure intensities, fluctuation velocity intensities, etc, are all bounded for asymptotical high Reynolds number, differing from the view of infinite logarithmic growth by [21] and references therein.

The turbulent Poiseuille flow between two parallel plates as shown in Fig.1 is one of the simplest possible physical situation, which has been studied intensively [1, 2]. Among those studies, someone adopt the Prandtl mixing length, such as Pomeau and Le Berre [15] studied the same problem with the Prandtl mixing length by taking into account boundary conditions: $\ell_{Pomeau}(0) = 0$, $\ell_{Pomeau}(2h) = 0$, and proposed mixing length as $\ell_{Pomeau} = \kappa y[1 - y/(2h)]$; and others use the Prandtl mixing length with damping function, such

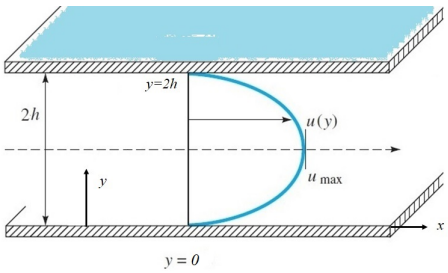

FIG. 1: Turbulent Poiseuille flow.

as Absi investigated the turbulent Poiseuille flow with a van Driest mixing length (combining the Prandtl mixing length ($\ell = \kappa y$) with damping function $[1-\exp(-y/A)]$), namely $\ell_{Absi} = \kappa y[1 - \exp(-y/A)]$, however this model is only valid for the wall at $y = 0$ but fails for the wall at $y = 2h$.

After validation, we found that both models [14, 15] are not able to provide a trustable prediction in the range of both buffer and sub-inertial. Therefore, it is still a great challenge to propose a mixing length model that can give an accurate predication in the whole domain of wall coordinates y, which is the task of this study.

The content of this paper is organised as follows, after introduction in Section 1; Section 2 propose an enhanced Prandtl-Driest mixing length; Section 3 completes formulations and find integration solutions and approximate analytical solution of mean motion; Section 4 calculates the turbulent viscosity, energy dissipation density and Kolmogorov scaling law; Section 5 presents the velocity fluctuations and total velocity field; Section 6 investigates the Reynolds stress and total shear stress; Section 7 constructs the moment of velocity fluctuation and ener-

Preprints (www.preprints.org) | NOT PEER-REVIEWED | Posted: 17 January 2022 doi:10.20944/preprints202201.0240.v1

gy balance; Section 8 obtains the friction of the turbulent Poiseuille flow between two parallel plates. Finally, a discussion is presented, and conclusions are drawn. As the essential part of this paper, a Maple code is provided.

II. AN ENHANCED PRANDTL-DRIEST MIXING LENGTH

We consider here a plane-parallel turbulent flow along an unbounded smooth plane surface (wall) as shown in Fig.1, and take the direction of the flow as the x axis and the plane of the surface as the xz plane, so y is the direction orthogonal to the surface. Assuming that the turbulent flow is steady with pressure gradient along the x axis, the y and z components of the mean velocity are zero, and all of the quantities depend only on y. The pressure gradient drives the against the shear stresses at the two walls.

According to the Prandtl mixing length theory [9], the Reynolds stress is proposed to be

$$\tau'_{xy} = -\rho\overline{u'v'} = \rho\ell^2|\frac{d\bar{u}}{dy}|\frac{d\bar{u}}{dy}, \tag{1}$$

where $\bar{u}$ is the mean velocity, μ is the dynamical viscosity, ρ is flow density, u' and v' are velocity fluctuation component. The mixing length ℓ must have length scale who should be a form that satisfy the boundary condition $\overline{u'v'} = 0$ at both bottom ($y = 0$) and top boundary ($y = 2h$), hence we can propose the mixing length as follows

$$\ell = \kappa y\varphi(y)\psi(y), \quad \varphi(0) = 0 \quad \text{and} \quad \varphi(2h) = 0. \tag{2}$$

where κ is a numerical constant, namely, the von Kármán constant, $\varphi(y)$ is a dimensionless function that may take different format. To satisfy the boundary condition, the function φ can be proposed to be

$$\varphi = (1 - \frac{y}{2h})^\gamma = \begin{cases} 0 & y = 0 \\ 0 & y = 2h \end{cases}, \tag{3}$$

where the parameter $\gamma > 0$, Prandtl [9] set $\gamma = 6/7$,; for simplicity, we set $\gamma = 1$ in this paper.

Regarding the determination of function $\psi(y)$, we need to take into account the fixed wall damping effects. We consider an infinite flat plate undergoing simple harmonic oscillation parallel to the plate in an infinite fluid. According to Stokes [32], the amplitude of the motion diminishes with increasing distance from the surface (wall) as a consequence of the bottom wall factor" $\psi_B = \exp(-\frac{y}{A})$" and top wall factor "$\psi_T = \exp(-\frac{2h-y}{A})$", where A is a constant depending the frequency of oscillation of the plate and kinematic viscosity ν of the fluid. Hence, in light of van Driest [26] we believe that when the plate is fixed and the fluid oscillates relative to the plate, the factor $[1-\exp(-y/A)][1-\exp(-\frac{2h-y}{A})]$ must be applied to the fluid oscillation to obtain the damping effect on the both bottom and top wall. Furthermore, van Driest pointed out that fully developed turbulent motion occurs only beyond a distance sufficiently remote from the wall, and eddies are not damped by the nearness of the wall. Indeed, near a wall, the damping factor is "$\psi = \psi_B\psi_T = [1-\exp(-y/A)][1-\exp(-\frac{2h-y}{A})]$" for each mean velocity fluctuation, and the Prandtl mixing length should be modified to the following

$$\ell = \kappa y\varphi\psi = \kappa y\varphi\psi_B\psi_T, \tag{4}$$

in order to take into account the mean motion all the way to a smooth wall, where the bottom wall van Driest damping function

$$\psi_B = [1 - \exp(-\frac{y}{A})], \tag{5}$$

and the top wall van Driest damping function

$$\psi_T = [1 - \exp(-\frac{2h - y}{A})]. \tag{6}$$

Introducing dimensionless parameters $\eta = yu_\tau/\nu$, $u^+ = \bar{u}/u_\tau$, $R_\tau = 2hu_\tau/\nu$, $A^+ = Au_\tau/\nu$ and friction velocity $u_\tau = \sqrt{\tau_w/\rho}$, we have dimensionless mixing length

$$\ell^+ = \kappa\eta\varphi^+\psi^+, \tag{7}$$

where

$$\varphi^+ = 1 - \frac{\eta}{R_\tau}, \tag{8}$$

$$\psi^+(\eta) = [1 - \exp(-\frac{\eta}{A^+})][1 - \exp(-\frac{R_\tau - \eta}{A^+})]. \tag{9}$$

The ℓ^+ in Eq.7 is the mixing length to be used in this paper, which is depicted in Fig.2

III. FORMULATIONS AND SOLUTIONS OF MEAN MOTION

The Reynolds-averaged Navier-Stokes equations [4] of the turbulent Poiseuille flow under pressure gradient, dp/dx, are reduced to

$$\rho\frac{d\overline{v'^2}}{dy} + \frac{\partial p}{\partial y} = 0, \tag{10}$$

$$\mu\frac{d^2\bar{u}}{dy^2} - \rho\frac{d\overline{u'v'}}{dy} - \frac{dp}{dx} = 0, \tag{11}$$

and boundary conditions as shown in Fig.1 and 3:

$$y = 0 : \bar{u} = 0, u' = 0, v' = 0, \text{ and } \mu\frac{d\bar{u}}{dy} = \tau_w, \tag{12}$$

Preprints (www.preprints.org) | NOT PEER-REVIEWED | Posted: 17 January 2022 doi:10.20944/preprints202201.0240.v1

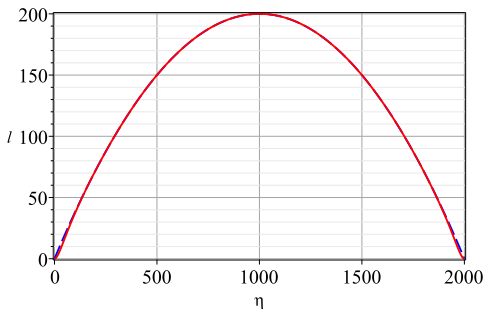

(a) The normal scale mixing length

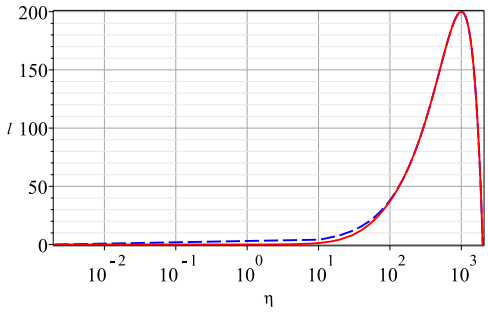

(b) The log rescale mixing length

FIG. 2: The normal and log-rescale of mixing length profile. Solid line is from Eq.7, and dashline is for mixing length without van Driest damping functions, namely $\kappa\eta(1-\eta/R_\tau)$.

and

$$y = 2h: \ \bar{u} = 0, \ u' = 0, \ v' = 0, \text{ and } \quad \mu\frac{d\bar{u}}{dy} = -\tau_w, \quad (13)$$

where $\bar{u}$ is the mean velocity, μ is the dynamical viscosity, ρ is flow density, p is pressure, u' and v' are velocity fluctuation component. The pressure gradient must be negative, namely $dp/dx < 0$, to maintain the flow motion. τ_w is the wall friction force on a unit area of the surface. This force is clearly in the x direction. The quantity τ_w is the constant flux of the x component of momentum transmitted by the fluid to the surface per unit time.

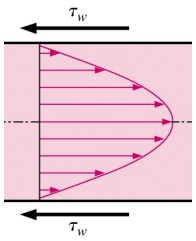

FIG. 3: Shear stress on the wall: $\tau_{xy}(y=0) = \tau_w$ and $\tau_{xy}(y = 2h) = -\tau_w$.

Integration of Eq.10 yields

$$\overline{v'^2} + \frac{p}{\rho} = \frac{p_0}{\rho}, \quad (14)$$

where p_0 is a function of x only [1]. Because $\overline{v'^2}$ is independent of x (by assumption), $\partial p/\partial x$ is equal to dp_0/dx. Both of these gradients should be independent of x to avoid streamwise acceleration of the flow. Eq.11 can be integrated to yield $\mu\frac{d\bar{u}}{dy} - \rho\overline{u'v'} = \frac{dp}{dx}y + C$. Applying the boundary condition in 13, we have $\overline{u'v'} = 0$ and leads to $C = \tau_w$. Hence we have governing equation as follows:

$$\nu\frac{d\bar{u}}{dy} - \overline{u'v'} = \frac{1}{\rho}\frac{dp_0}{dx}y + \frac{\tau_w}{\rho}, \quad (15)$$

where $\nu = \mu/\rho$ is kinematic viscosity. Applying the boundary condition in 13, we have the relation between the wall friction and the pressure gradient:

$$\frac{dp_0}{dx} = -\frac{\tau_w}{h}, \quad (16)$$

which indicate that the shear stress at the wall is determined by the pressure gradient and width of the channel only, which is one reason why this flow is less complicated than others [1]. Hence the Eq.15 is rewritten as

$$\nu\frac{d\bar{u}}{dy} - \overline{u'v'} = \frac{\tau_w}{\rho}(1 - \frac{y}{h}). \quad (17)$$

The first term on the left-hand side of Eq. 17 represents the effect of viscosity on the mean flow, whereas the second term is the Reynolds stress, namely $\tau'_{xy} = -\rho\overline{u'v'}$. In turbulent flow located some distance away from a wall, the Reynolds stress is of considerably greater magnitude than the viscous stress; however, the role of viscous stress increases as the distance to a smooth wall decreases until finally, at the wall, viscosity predominates.

Using the mixing length in Eq.2, Eq. 17 becomes $\nu\frac{d\bar{u}}{dy} + (\kappa y\varphi\psi)^2|\frac{d\bar{u}}{dy}|\frac{d\bar{u}}{dy} = \frac{\tau_w}{\rho}(1 - \frac{y}{h})$, which has two formats for different domain of y and each of them has its own solution.

(a) In the domain $y \in [0, h]$, we have $\frac{d\bar{u}}{dy}>0$, the governing equation is

$$\nu\frac{d\bar{u}}{dy} + \ell^2(\frac{d\bar{u}}{dy})^2 = \frac{\tau_w}{\rho}(1 - \frac{y}{h}), \quad (18)$$

(b) In the domain $y \in [h, 2h]$, we have $\frac{d\bar{u}}{dy}<0$, the governing equation is

$$\nu\frac{d\bar{u}}{dy} - \ell^2(\frac{d\bar{u}}{dy})^2 = \frac{\tau_w}{\rho}(1 - \frac{y}{h}). \quad (19)$$

With the dimensionless quantities, Eq.1 can be expressed as

$$\frac{\tau'_{xy}}{\rho u_\tau^2} = (\ell^+)^2|\frac{du^+}{d\eta}|\frac{du^+}{d\eta}, \quad (20)$$

and Eq. 18 can be rewritten as

$$\frac{du^+}{d\eta} + (\ell^+)^2\left(\frac{du^+}{d\eta}\right)^2 = 1 - \frac{2\eta}{R_\tau}, \quad \eta \in [0, \frac{R_\tau}{2}], \quad (21)$$

Preprints (www.preprints.org) | NOT PEER-REVIEWED | Posted: 17 January 2022 doi:10.20944/preprints202201.0240.v1

and the boundary condition

$$\eta = 0 : \ u^+ = 0. \tag{22}$$

The solution of Eq.21 valid in whole domain of η has never been obtained while only asymptotic solutions have been proposed [1, 2], which caused a buffer problem between segmental solutions.

From Eq.21, we can obtain

$$\frac{du^+}{d\eta} = \frac{2(1-\frac{2\eta}{R_\tau})}{1+\sqrt{1+4(\ell^+)^2(1-\frac{2\eta}{R_\tau})}}. \tag{23}$$

hence the singularity-free solution is

$$u^+ = \int \frac{2(1-\frac{2\eta}{R_\tau})}{1+\sqrt{1+4(\ell^+)^2 2(1-\frac{2\eta}{R_\tau})}} d\eta. \tag{24}$$

Similarly, Eq. 19 can be rewritten as

$$\frac{du^+}{d\eta} - (\ell^+)^2 \left(\frac{du^+}{d\eta}\right)^2 = 1 - \frac{2\eta}{R_\tau}, \quad \eta \in [\frac{R_\tau}{2}, R_\tau], \tag{25}$$

and the boundary condition

$$\eta = R_\tau : \ u^+ = 0, \tag{26}$$

From Eq.25, we can obtain

$$\frac{du^+}{d\eta} = \frac{2(1-\frac{2\eta}{R_\tau})}{1+\sqrt{1-4(\ell^+)^2(1-\frac{2\eta}{R_\tau})}}. \tag{27}$$

hence the singularity-free solution is

$$u^+ = \int \frac{2(1-\frac{2\eta}{R_\tau})}{1+\sqrt{1-4(\ell^+)^2(1-\frac{2\eta}{R_\tau})}} d\eta. \tag{28}$$

We can combine the derivatives in Eqs. (23), (27) into a single from below:

$$\frac{du^+}{d\eta} = \frac{2(1-\frac{2\eta}{R_\tau})}{1+\sqrt{1-4(\ell^+)^2 \mid (1-\frac{2\eta}{R_\tau}) \mid}}, \quad \eta \in [0, R_\tau], \tag{29}$$

which is depicted in Fig. 4. It shows that the velocity gradient is enormous near the wall, but decay rapidly to almost zero as away from the wall. That is why the velocity profile near the wall must be obtained if we wish have a better understanding of turbulence boundary layer.

We can also combine the integral solutions in Eqs.(24) and (28 into a single from as follows:

$$u^+ = \int \frac{2(1-\frac{2\eta}{R_\tau})}{1+\sqrt{1+4(\ell^+)^2 \mid (1-\frac{2\eta}{R_\tau}) \mid}} d\eta, \tag{30}$$

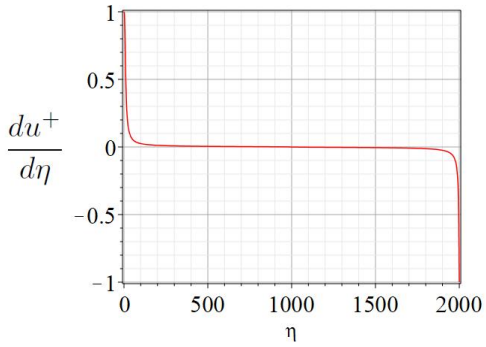

(a) The normal scale velocity gradient profile

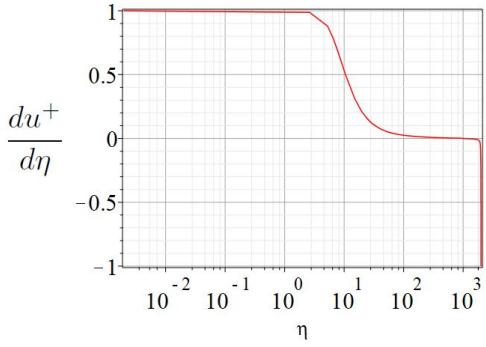

(b) The log rescale velocity gradient profile

FIG. 4: The normal scale and log-rescale of flow velocity gradient profile of turbulent Poiseuille flow.

To the best of the author's knowledge, the above integrations in the integral (30) can not be completed exactly but approximately. One solution can be integrated by parts, yields

$$u^+ = \sum_{n=1}^{\infty} \frac{(-1)^n}{n!} \eta^n \frac{d^n u^+}{d\eta^n}, \tag{31}$$

where $\frac{du^+}{d\eta} = \frac{2(1-\frac{2\eta}{R_\tau})}{1+\sqrt{1-4(\ell^+)^2|(1-\frac{2\eta}{R_\tau})|}}$, and $\frac{d^2u^+}{d\eta^2} = \frac{d}{d\eta}(\frac{du^+}{d\eta}),.., \frac{d^n u^+}{d\eta^n} = \frac{d}{d\eta}(\frac{d^{n-1}u^+}{d\eta^{n-1}})$. This series solution can be computed to any order, however the series' convergence is poor and will need many terms to have a log law trends, we will not going to use this series solution in our computation.

Numerically the integral (30) can be easily work out, the author wrote a Maple code to compute the integral, the result is depicted in Fig. 5. It shows that the flow velocity is rapidly increase as away from the wall and decrease as close to the center of the channel.

It is worth to note that the log rescale mean velocity has a nice high heels profile because of taking into account the boundary conditions of both walls. You would"nt see the high heels profile if you only consider one wall. This high heels profile has never been seen in the literature and is a universal feature of bounded flows.

Preprints (www.preprints.org) | NOT PEER-REVIEWED | Posted: 17 January 2022 doi:10.20944/preprints202201.0240.v1

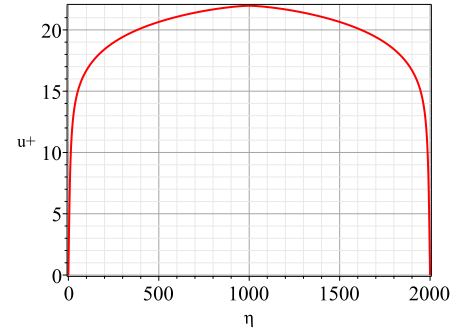

(a) The normal scale velocity profile

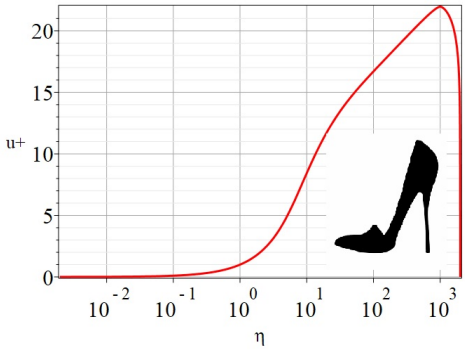

(b) The log rescale velocity high heels profile

FIG. 5: The normal scale and log-rescale of flow velocity profile of turbulent Poiseuille flow.The Maple code of the solution: $u^+(a)$=int($\frac{du^+}{d\eta}$,eta=0..a,numeric).

Although the integral (30) can not be completed exactly, we can try to get a approximate analytical solution. In light of author's previous work [30], which obtained a closed form solution for plane turbulent flow and proposed an approximate analytical solution, we can propose an solution as follows

$$u^+ \approx \frac{1}{\kappa}\ln\left[2\ell_C^+ + \sqrt{1+4(\ell_C^+)^2}\right] + \frac{\beta\ell_C^+}{1+\sqrt{1+4(\ell_C^+)^2}}, \quad \eta\in[0,R_\tau], \tag{32}$$

where

$$\ell_C^+ = \kappa\eta\varphi^+\psi_C^+, \quad (C,\beta)=(9,9) \quad \text{or} \quad (C,\beta)=(26,8.8)$$
$$\psi_C^+ = [1-\exp(-\frac{\eta}{C})][1-\exp(-\frac{R_\tau-\eta}{C})], \tag{33}$$

This approximated analytical solution is valid in whole domain $\eta\in[0,R_\tau]$, and has not been seen in the literature.

The solution of Eq. 24, Eq.28 and Eq. 32 are depicted in Figs. 6 and its log-rescale–the high heels velocity profile. It is remarkable to see that both the numerical integral solution and approximate analytical solution are perfectly agree with both DNS solutions [23, 24] and experiments [25] in the domain of $\eta\in[0,\ R_\tau/2]$. They do not have data in another half domain $[R_\tau/2,\ R_\tau]$, hence their curve are open rather than close as us.

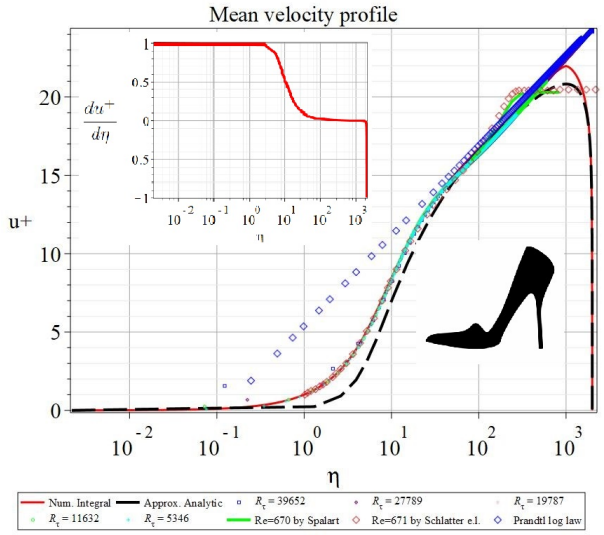

(a) The log rescale mean velocity.

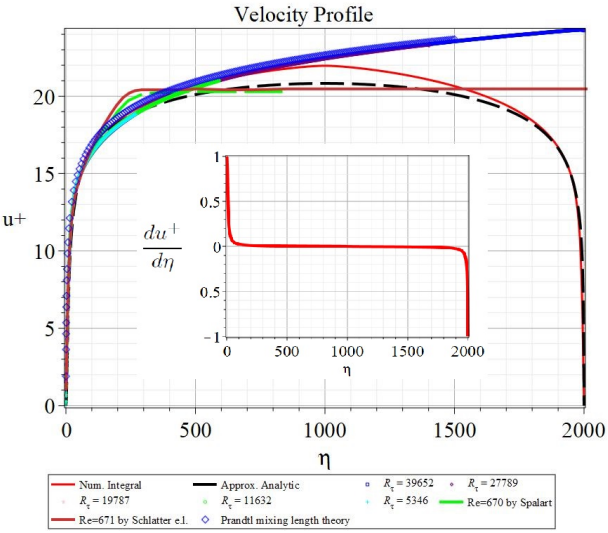

(b) The normal scale mean velocity.

FIG. 6: The log-rescale high heels velocity profile of turbulent Poiseuille flow and comparisons: the numerical integration solution, the approximate analytical solution, the direct numerical simulation (DNS) solutions [23, 24] and experiments (all data with R_τ)[25] .

IV. THE TURBULENT VISCOSITY, ENERGY DISSIPATION DENSITY AND KOLMOGOROV SCALING LAW

The turbulent viscosity is $\nu_T = (\kappa y)^2(1-\frac{y}{2h})^2|\frac{d\bar{u}}{dy}| = \nu\kappa^2\eta^2(1-\frac{\eta}{R_\tau})^2|\frac{du^+}{d\eta}|$, where $\frac{du^+}{d\eta} =$

Preprints (www.preprints.org) | NOT PEER-REVIEWED | Posted: 17 January 2022 doi:10.20944/preprints202201.0240.v1

$\frac{2(1-\frac{2\eta}{R_\tau})}{1+\sqrt{1+4\kappa^2\eta^2(\varphi^+\psi^+)^2|(1-\frac{2\eta}{R_\tau})|}}$; hence,

$$\nu_T = \frac{2\nu\kappa^2\eta^2(1-\frac{\eta}{R_\tau})^2|(1-\frac{2\eta}{R_\tau})|}{1+\sqrt{1+4\kappa^2\eta^2(\varphi^+\psi^+)^2 \mid (1-\frac{2\eta}{R_\tau}) \mid}}. \quad (34)$$

This relation reveals that the turbulent viscosity is not constant but rather changes with η. It is depicted in Fig. 7.

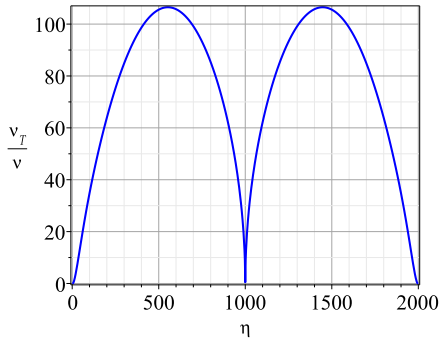

(a) The normal scale turbulent viscosity ratio

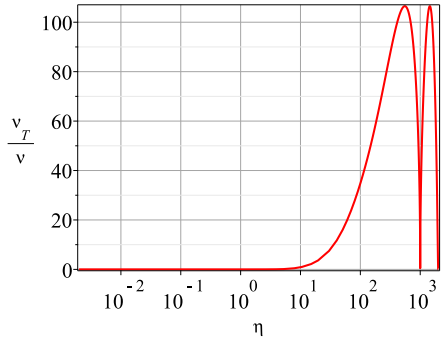

(b) The log rescale turbulent viscosity ratio

FIG. 7: The turbulent viscosity ratio.

.

According to Landau [3], the mean energy flux density is $< q >= \bar{u}\tau_w$, and the energy dissipation density in the turbulent flow is

$$\varepsilon = \frac{1}{\rho}\frac{d < q >}{dy} = \frac{1}{\nu}(\frac{\tau_w}{\rho})^2\frac{du^+}{d\eta} = \frac{u_\tau^4}{\nu}\frac{du^+}{d\eta}$$
$$= \frac{u_\tau^4}{\nu}\frac{2(1-\frac{2\eta}{R_\tau})}{1+\sqrt{1+4\kappa^2\eta^2(\varphi^+\psi^+)^2 \mid (1-\frac{2\eta}{R_\tau}) \mid}}, \quad (35)$$

which gives $\lim_{\eta\to 0}\varepsilon = \frac{u_\tau^4}{\nu}$, i.e., a power law u_τ^4; in contrast, Landau's energy dissipation density [3], $\varepsilon_{\text{Landau}} = (\frac{\tau_w}{\rho})^{3/2}\frac{1}{\kappa y} = \frac{u_\tau^4}{\nu}\frac{1}{\kappa\eta}$, is infinite at the surface $\eta = 0$, indicating that maintaining turbulent flow requires supplying an infinite energy source, which is physically impossible. The energy dissipation density ratio $\epsilon = \frac{\varepsilon\nu}{u_\tau^4}$ is depicted in Fig.8.

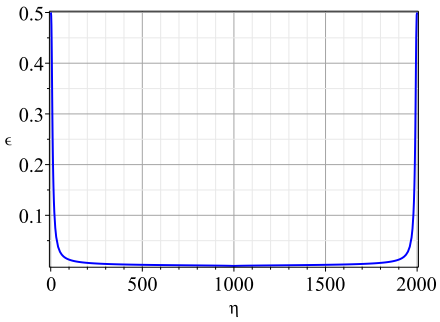

(a) The normal scale of the energy dissipation density ratio

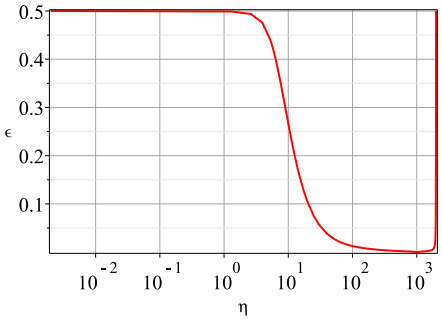

(b) The normal scale of the energy dissipation density ratio

FIG. 8: The energy dissipation density ratio $\epsilon = \frac{\varepsilon\nu}{u_\tau^4}$ decreases to null rapidly as η increases away from the surface.

According to Kolmogorov [28, 33–35], we have $E(k) = 1.5\varepsilon^{2/3}k^{-5/3}$, namely,

$$E(k) = \frac{1.5\nu^{-2/3}k^{-5/3}u_\tau^{8/3}[2(1-\frac{\eta}{R_\tau})]^{2/3}}{\left(1+\sqrt{1+4\kappa^2\eta^2(\varphi^+\psi^+)^2 \mid (1-\frac{2\eta}{R_\tau}) \mid}\right)^{2/3}}, \quad (36)$$

where $E(k)$ is the kinetic energy per unit mass of fluid in eddies with wave number k. Hence, at the surface $\eta = 0$, we have $E(k)_{\eta=0} = 1.5u_\tau^{8/3}k^{-5/3}\nu^{-2/3}$. $\Sigma = \frac{E}{1.5\nu^{-2/3}k^{-5/3}u_\tau^{8/3}}$ is depicted in Fig.9, which shows that the turbulent energy dissipation is mainly concentrated in a narrow region close to the boundary surface and decays rapidly away from the surface.

V. THE VELOCITY FLUCTUATIONS AND TOTAL VELOCITY FIELD

In Prandtl mixing length theory [2, 9], Prandtl assumes a great simplified model of the fluctuations, according to which the individual fluid elements are displaced in a mean distance (the mixing length) ℓ by the fluctuations, perpenticular to the main flow direction, but still retain their momentum. The element that was initially at y, and is now at $y+\ell$, has a higher velocity than its new surrendings. The velocity difference is a measure of the

Preprints (www.preprints.org) | NOT PEER-REVIEWED | Posted: 17 January 2022 doi:10.20944/preprints202201.0240.v1

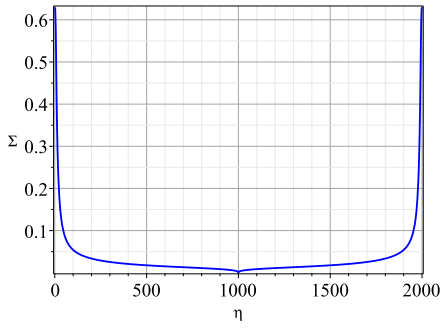

(a) The normal scale of the kinetic energy ratio

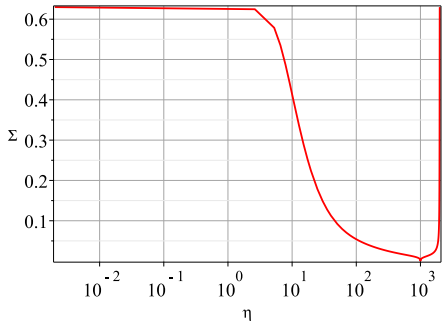

(b) The log rescale of the kinetic energy ratio

FIG. 9: The kinetic energy ratio $\Sigma(\eta) = \frac{E}{1.5\nu^{-2/3}k^{-5/3}u_\tau^{8/3}}$

fluctuation velocity in the x direction:

$$\Delta u = \bar{u}(y+\ell) - \bar{u}(y) \approx \ell \frac{d\bar{u}}{dy}. \tag{37}$$

Prandtl assumed that the velocity fluctuation component v' is the same order of magnitude as u', namely $v' \sim u'$, therefore we have

$$v' = \alpha \ell \frac{d\bar{u}}{dy}. \tag{38}$$

where $\alpha \approx 1/\sqrt{2}$ is introduced by the calculation of [36] and in page 528 of [2].

Using dimensionless quantities and $\frac{du^+}{d\eta} = \frac{2(1-\frac{2\eta}{R_\tau})}{1+\sqrt{1+4(\ell^+)^2|(1-\frac{2\eta}{R_\tau})|}}$, we have $u'^+ \equiv u'/u_\tau = \ell^+ \frac{d\bar{u}^+}{d\eta}$ and $v'^+ \equiv v'/u_\tau = \alpha \ell^+ \frac{d\bar{u}^+}{d\eta}$, namely

$$u'^+ = \frac{2\ell^+|(1-\frac{2\eta}{R_\tau})|}{1+\sqrt{1+4(\ell^+)^2 \mid (1-\frac{2\eta}{R_\tau}) \mid}}, \tag{39}$$

$$v'^+ = \frac{\sqrt{2}\ell^+|(1-\frac{2\eta}{R_\tau})|}{1+\sqrt{1+4(\ell^+)^2 \mid (1-\frac{2\eta}{R_\tau}) \mid}}, \tag{40}$$

where the symmetry of fluctuations about $\eta = R_\tau/2$ has been applied. The fluctuations u'^+ or v'^+ are depicted in Fig.10.

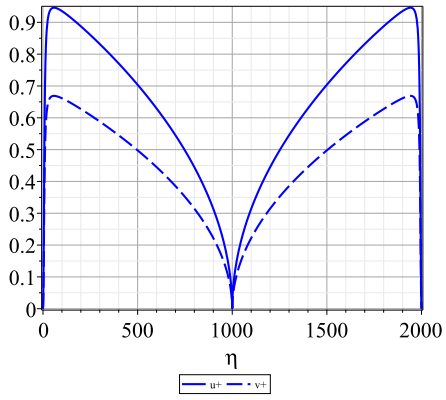

(a) The normal scale velocity fluctuations

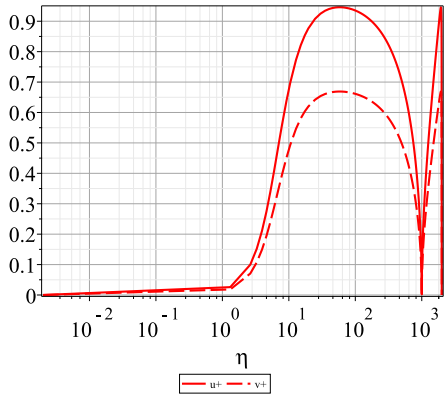

(b) The log rescale velocity fluctuations

FIG. 10: Flow velocity fluctuations, where Φ stands for either u'^+ or v'^+

We can verify both velocity fluctuations are satisfy the Reynolds-averaged conditions $\overline{u'^+} = 0$ and $\overline{v'^+} = 0$. Since the problem is steady flow and now the Reynolds-averaged conditions of quantity Φ is defined as follows

$$\overline{\Phi'^+} = \frac{1}{R_\tau}\int_0^{R_\tau} \Phi d\eta. \tag{41}$$

Substituting Eqs.39 and 40, can prove this statement. Alternatively, prove it by numerical integral, for instance using Maple code: int(u'^+, $\eta = 0..R_\tau$,nemeric) yields null, which can be interpreted easily because of the asymmetry of the velocity fluctuations about $y = R_\tau/2$.

With the mean velocity and fluctuations, we have the total flow velocity components U and V in x and y direction, respectively.

$$U^+ = u^+ + u'^+, \tag{42}$$

$$V^+ = v'^+, \tag{43}$$

since $\bar{v}$ is assumed to be zero, where U^+U/u_τ and $V^+ = V/u_\tau$. The total flow velocity U^+ and mean velocity u^+ are depicted in Fig.11.

Preprints (www.preprints.org) | NOT PEER-REVIEWED | Posted: 17 January 2022 doi:10.20944/preprints202201.0240.v1

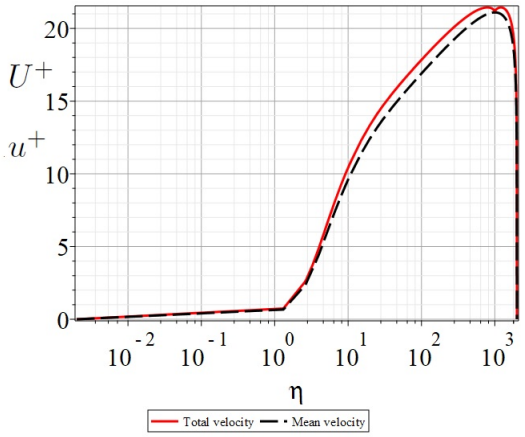

FIG. 11: Total flow velocity has a high heels profile and is slight larger than the mean velocity due to the contribution of the fluctuations.

VI. REYNOLDS STRESS AND TOTAL SHEAR STRESS

The Reynolds stress is given by $\tau'_{xy} = \rho u_\tau^2 \kappa^2 \eta^2 (\varphi^+ \psi^+)^2 |\frac{du^+}{d\eta}| \frac{du^+}{d\eta}$. The Reynolds stress ratio $\frac{\tau'_{xy}}{\rho u_\tau^2}$ is depicted in Fig. 12.

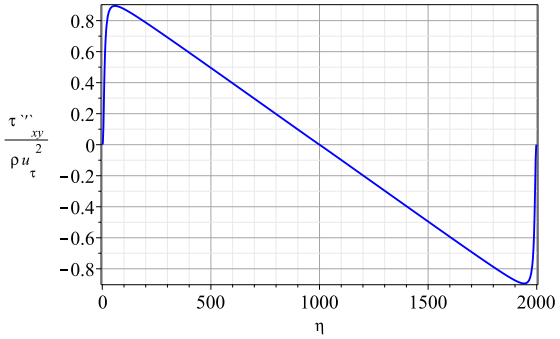

(a) The normal scale of the Reynolds stress ratio

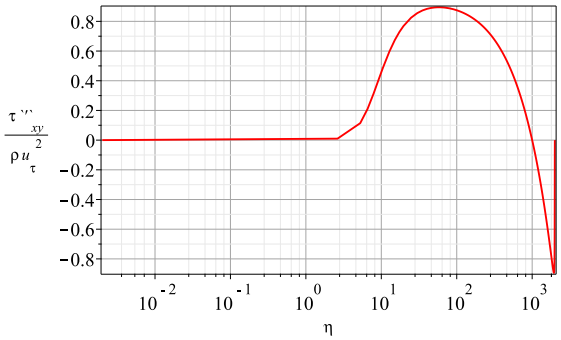

(b) The log rescale of the Reynolds stress ratio

FIG. 12: The Reynolds stress ratio $\frac{\tau'_{xy}}{\rho u_\tau^2}$.

Total shear stress is given by $\tau_{xy} = \mu \frac{d\bar{u}}{dy} + \tau'_{xy}$, namely

$$\tau_{xy} = \tau_w \left(1 + (\ell^+)^2 |\frac{du^+}{d\eta}|\right) \frac{du^+}{d\eta}, \tag{44}$$

where $\tau_w = \rho u_\tau^2$. The total shear stress is depicted in Fig. 13.

which is depicted in Fig.13.

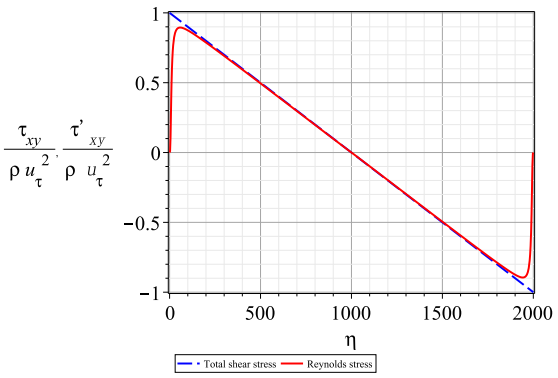

(a) The normal scale total shear stress

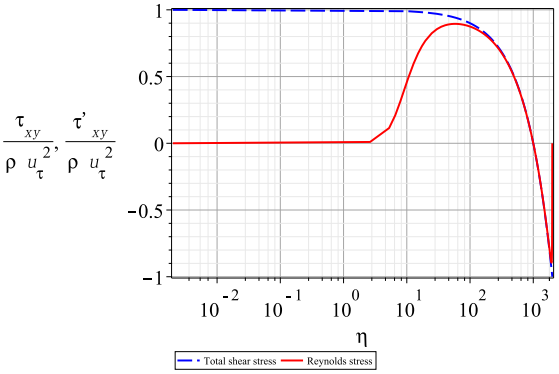

(b) The log rescale total shear stress

FIG. 13: Total shear stress and the Reynolds stress.

The Fig.13 reveals that only difference in between are near the walls, away from the walls, they are almost equal.

VII. THE MOMENT OF VELOCITY FLUCTUATION AND ENERGY BALANCE

The square of the streamwise flow velocity fluctuation with the wall distance, i.e., $\overline{(u'^+)^2}$ is given by

$$\overline{(u'^+)^2} = \frac{4(\ell^+)^2(1-\frac{2\eta}{R_\tau})^2}{\left(1+\sqrt{1+4(\ell^+)^2\,|\,(1-\frac{2\eta}{R_\tau})\,|}\right)^2}, \tag{45}$$

and $\overline{(v'^+)^2}$ as follows

$$\overline{(v'^+)^2} = \frac{2(\ell^+)^2(1-\frac{2\eta}{R_\tau})^2}{\left(1+\sqrt{1+4(\ell^+)^2\,|\,(1-\frac{2\eta}{R_\tau})\,|}\right)^2}. \tag{46}$$

Preprints (www.preprints.org) | NOT PEER-REVIEWED | Posted: 17 January 2022 doi:10.20944/preprints202201.0240.v1

Both $\overline{(u'^+)^2}$ and $\overline{(v'^+)^2}$ have similar profile as in Fig.14 and their square root $\sqrt{\overline{(u'^+)^2}}$ and $\sqrt{\overline{(v'^+)^2}}$ are shown

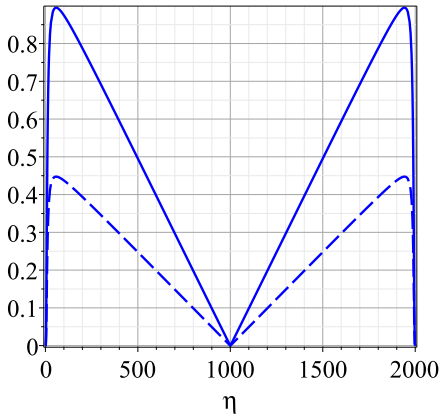

(a) The normal scale of $\overline{(u'^+)^2}$ (solid) and $\overline{(v'^+)^2}$ (dash).

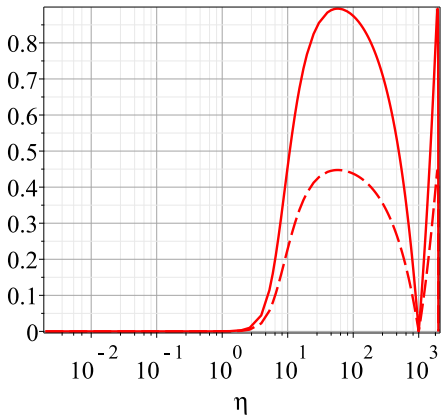

(b) The log rescale of $\overline{(u'^+)^2}$ (solid) and $\overline{(v'^+)^2}$ (dash).

FIG. 14: The square moment: $\overline{(u'^+)^2}$ or $\overline{(v'^+)^2}$.

in Fig.15

The energy balance equation can be be derived from the momentum balance equation as follows:

$$\underbrace{(1-\frac{2\eta}{R_\tau})\frac{du+}{d\eta}}_{E_{es}} = \underbrace{\left(\frac{du+}{d\eta}\right)^2}_{E_{dd}} + \underbrace{(\ell^+)^2\left(\frac{du+}{d\eta}\right)^3}_{E_{tp}}, \qquad (47)$$

where E_{es} is energy supply, E_{dd} is direct dissipation, and E_{tp} is turbulence production. They are depicted in Fig.16

The energy balance in Eq.16 reveals that the power due to the shear forces is divided into two parts. One is transformed directly to internal energy via viscous dissipation (E_{dd}) while the 2nd is used to generate turbulent fluctuation energy (E_{tp}).

The turbulence production has a maximum of 0.2447 at $\eta = 10.46$. At this distance from the wall, the direct dissipation and the turbulence production are equal. For $\eta < 10.46$ the direct dissipation dominates, and for $\eta > 10.46$ the entire energy supply eventually provides the

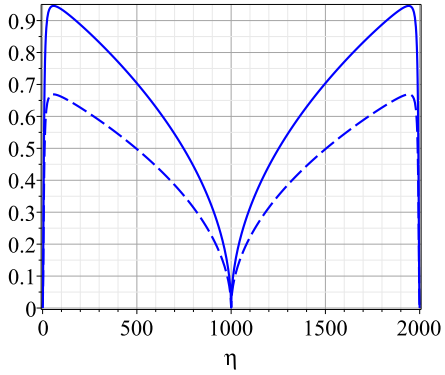

(a) The normal scale of $\sqrt{\overline{(u'^+)^2}}$ (solid) and $\sqrt{\overline{(v'^+)^2}}$ (dash).

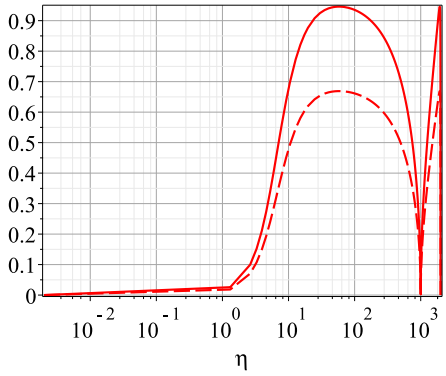

(b) The log rescale of $\sqrt{\overline{(u'^+)^2}}$ (solid) and $\sqrt{\overline{(v'^+)^2}}$ (dash).

FIG. 15: The square root: $\sqrt{\overline{(u'^+)^2}}$ or $\sqrt{\overline{(v'^+)^2}}$.

turbulence production as $\eta \to R_\tau/2$, namely closing the center of the channel [2]

The energy balance of the turbulent fluctuations can also be obtained and shown in Fig.17.

VIII. FRICTION OF THE TURBULENT POISEUILLE FLOW BETWEEN TWO PARALLEL PLATES

As an application of our solutions, let us now to construct the dependence of the resistance coefficient, which is defined as $\lambda = \frac{2h\Delta p/l}{(1/2)\rho\bar{u}^2} = 2h\frac{2\rho u_\tau^2}{h}/(\rho\bar{u}^2/2) = 8(u_\tau/\bar{u})^2 = 8/(u^+)^2$, which gives

$$u^+ = \sqrt{\frac{8}{\lambda}}. \qquad (48)$$

The dimensionless Reynolds number is defined as $Re = 2h\bar{u}/\nu = (2hu_\tau/\nu)u^+$, hence $\eta|_{y=2h} = 2hu_\tau/\nu = 2h(\bar{u}/u_\tau)/\nu = Re/(2u^+)$ and $2\kappa\eta|_{y=2h} = \kappa Re/u^+$. Applying the Eq.48 into the above relation, and leads to

$$\eta_h \equiv \eta|_{y=2h} = \frac{1}{2}Re\sqrt{\frac{\lambda}{8}}. \qquad (49)$$

Preprints (www.preprints.org) | NOT PEER-REVIEWED | Posted: 17 January 2022 doi:10.20944/preprints202201.0240.v1

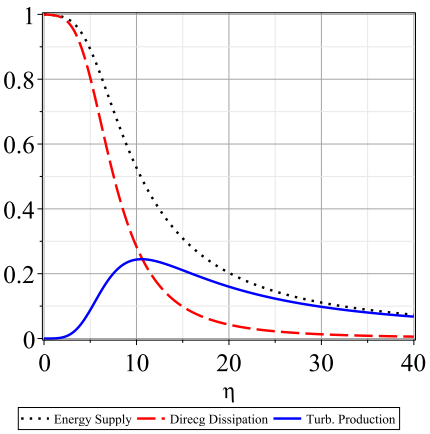

(a) The normal scale profile

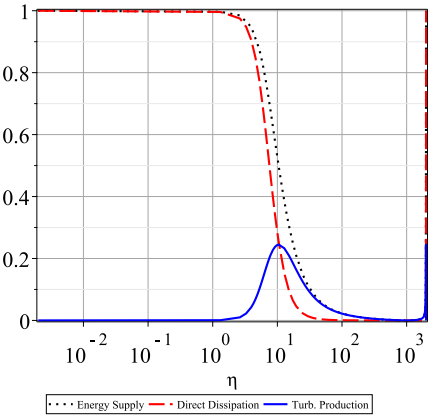

(b) The log rescale profile

FIG. 16: Universal energy balance of the mean motion.

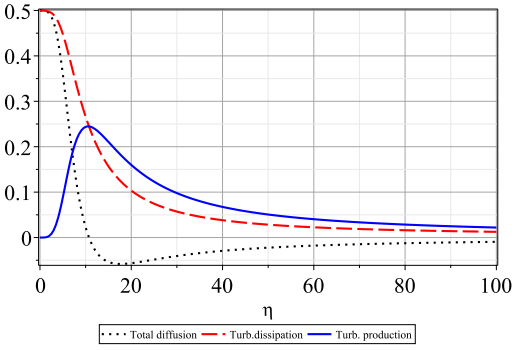

FIG. 17: Universal energy balance of the turbulent fluctuations: Turbulence production +Total diffusion=Turbulent dissipation.

The dependence of the resistance coefficient on the dimensionless Reynolds Re number is given in implicit form by the equation

$$\sqrt{\frac{8}{\lambda}} = \frac{1}{\kappa}\ln\left(2\ell_h + \sqrt{(2\ell_h)^2+1}\right) + \frac{\beta\ell_h}{1+\sqrt{(2\ell_h)^2+1}} \tag{50}$$

where

$$\ell_h = \kappa\eta_h(1-\frac{\eta_h}{R_\tau})[1-\exp(-\frac{\eta_h}{C})][1-\exp(-\frac{R_\tau-\eta_h}{C}] \tag{51}$$

Eq. 50 and the Prandtl log-law, $1/\sqrt{\lambda} = 2\log(Re\sqrt{\lambda}) - 0.8$, and others are depicted in Fig. 18.

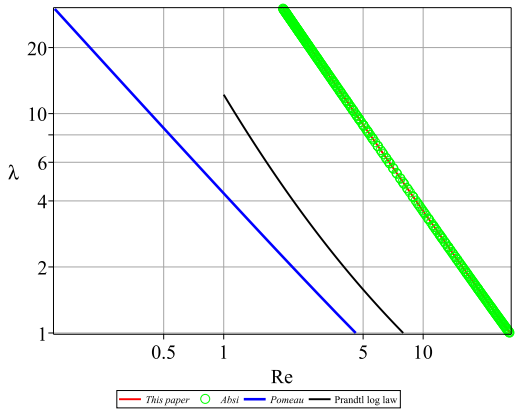

FIG. 18: Resistance coefficient of the turbulent Poiseuille flow between two parallel plates.

IX. CONCLUSIONS

To the best of the author's knowledge, the enhanced mixing length is the first complete model be ever proposed to consider both walls boundary conditions. The study shown that the high heels mean and total motion profile is universal for all wall-bounded turbulent flows. The explicit approximate analytical solutions, the total velocity, the total shear stress and the friction of turbulent Poiseuille flow between two parallel plates have not be seen in literature before. The investigation confirmed that the correct mixing length formulae must include all boundary condition together with damping functions by multiplication. This study may help to have a better understanding of turbulence phenomena [27–31].

ACKNOWLEDGMENTS

This work was supported by Xi'an University of Architecture and Technology (Grant No. 002/2040221134). The author wishes to express his appreciation to Prof. X. Chen from Beihang University for providing some useful

publications and to Mr. Zhe Liu for extracting the DNS and experimental data from Refs: [23–25], which are used to draw Fig. 6.

Availability of data

The data supporting the findings of this study are available from the corresponding author upon reasonable request.

Interest Conflict

The author declare that they have no conflict of interest.

[1] H. Tennekes and J.L. Lumley, A First Course of Turbulence, The MIT Press, Cambridge (1972).

[2] H. Schlichting, Boundary Layer Theory, fourth ed., McGraw-Hills, 1960 translated by J. Kestin.

[3] L.D. Landau and E. M. Lifshitz, *Fluid Mechanics* (2nd ed.) (Butterworth-Heinemann, 1987).

[4] O. Reynolds, On the dynamical theory of incompressible viscous fluids and the determination of the criterion. Philosophical Transactions of the Royal Society of London. 1895;186, 123-164. https://doi.org/10.1098/rsta.1895.0004

[5] L. Prandtl, On fluid motions with very small friction (in german). *Third International Mathematical Congress, Heidelberg (1904)*

[6] H. Blasius, Grenzschichten in Fljssigkeiten mit kleiner Reibung. *Z. Math. Phys.*, **56**(1908) 1-37.

[7] L. Prandtl, Bemerkungen über die entstehung der turbulenz, *Z. Angew. Math. Mech.* **1**(1921):431-436.

[8] Th. von Kármán, Über leminere und turbulence Reibung (On Laminer and Turbulent Friction), *Z. Angew. Math. Mech.* **1** (1921)223.

[9] L. Prandtl, Bericht über Untersuchungen zur ausgebildeten Turbulenz, *Z. Angew. Math. Mech.* **5**(2)(1925)136-139.

[10] C. M. Millikan, A critical discussion of turbulent flows in channels and circular tubes, in *Proceedings of the Fifth International Congress for Applied Mechanics*, Harvard University and MIT, 1938 (Wiley, New York, 1939).

[11] J. Nikuradse, Untersuchungen über turbulente Strömungen in nicht kreisförmigen Rohren. *Ing. Arch* **1**(1930) 306-332.

[12] J. Nikuradse, Gesetzmässigkeiten der turbulenten Stromung in glatten Rohren, *Forschung auf dem Gebiet des Ingenieurwesens A* (1934) 44.

[13] R. Baidya, J. Philip, N. Hutchins, J. P. Monty, and I. Marusic, Distance-from-the-wall scaling of turbulent motions in wall-bounded flows, *Phy.Fluids* **29**(2017) 020712.

[14] R. Absi, A simple eddy visosity formulation for turbulent boundat payers near smooth walls, C.R. Mecanique, 337(2009)158-165.

[15] Y. Pomeau and M. Le Berre, Turbulent plane Poiseille flow, EPJ, 2021.

[16] Z.S. She, X. Chen and F. Hussain, Quantifying wall turbulence via a symmetry approach: A Lie group theory, J. Fluid, Mech.827:322-356 (2017).

[17] B.J. Cantwell, A universal velocity profile for smooth wall pipe flow, J. Fluid Mech.,878:834-874(2019).

[18] X. Chen, X, F. Hussain and Z. S. She, Quantifying wall turbulence via a symmetry approach: Part II. Reynolds stresses, J. Fluid Mech. 850: 401-438 (2018).

[19] X. Chen and SK.R. reenivasan, Reynolds number scaling of the peak turbulence intensity in wall flows, J. Fluid Mech., 908,R3 (2021)

[20] X. Chen and SK.R. reenivasan, Law of bounded dissipation and its consequences in turbulent wall flows, J. Fluid Mech., 933,A30(22)

[21] I. Marusic, W.J. Baars and N. Hutchins, Scaling of the streamwise turbulence intensity in the context of inner-outer interactions in wall turbulence, Phys. Rev. Fluids, 2, 100502(2017)

[22] P. Luchini, Universality of the turbulent velocity profile, *Phys.Rev.Lett.* **118**(2017) 224501.

[23] P. Schlatter, R. Örlü, Q. Li, G. Brethouwer, J.H.M. Fransson, A.V. Johnsson, P.H. Alfredsson and D.S. Henningson, Turbulent boundary layers up to $Re_\theta = 2500$ studied through simulation and experiment. *Phys. Fluids* **21**(2019) 051702.

[24] P. R. Spalart, Direct simulation of a turbulent boundary layer up to $R_\theta = 1410$, *J. Fluid Mech.* **187** (1988)61-98.

[25] Willert, C., Soria, J., Stanilas, M., Klinner, J., Amili, O., Eisfelder, M., Cuvier, C., Bellani, G., Fiorini, T. & Talamelli, A. 2017 Near-wall statistics of a turbulent pipe flow at shear Reynolds numbers up to 40 000. J. Fluid Mech. 826, R5.

[26] E.R. van Driest, On turbulent flow near a wall. *J. Aeronaut. Sci.* (Institute of the Aeronautical Sciences) **23**(11)(1956) 1007 – 1011 .

[27] B. H. Sun, The temporal scaling laws of compressible turbulence, *Modern Physics Letters B*, **30**(23)(2016) 1650297 (14 pages).

[28] B. H. Sun, Scaling laws of compressible turbulence, *Appl. Math. Mech.* -Engl. Ed., **38**(6)(2017) 765-778.

[29] B. H. Sun, Thirty years of turbulence study in China. *Applied Mathematics and Mechanics*, **40**(2)(2019) 193-214.

[30] B. H. Sun, Revisiting the Reynolds-averaged Navier-Stokes equations, *Open Physics* **19** (2021) 853-862.

[31] B. H. Sun, Closed Form Solution of Plane-Parallel Turbulent Flow Along an Unbounded Plane Surface. *Preprints* (2021) 2021110008 (doi:

10.20944/preprints202111.0008.v3); Fractals - Complex Geometry, Patterns, and Scaling in Nature and Society (accepted).

[32] G. G. Stokes, On the effect of the internal friction of fluids on the motion of pendulums, *Trans. Cambridge Philos. Soc.*, **9** (1851).

[33] A. N. Kolmogorov, The local structure of turbulence in incompressible viscous fluid for very large Reynolds number. *Dokl. Akad. Nauk SSSR*, **30**(1941), 299-303 (reprinted in *Proc.R.Soc.Lond.* A, **434**(1991)9-13.)

[34] A. N. Kolmogorov, On degeneration (decay) of isotropic turbulence in an incompressible visous liquid. *Dokl. Akad. Nauk SSSR*, **31**(1941) 538-540.

[35] A. N. Kolmogorov, Dissipation of energy in locally isotropic turbulence. *Dokl.Akad. Nauk SSSR.*, **32**(1941) 16-18 .(reprinted in *Proc.R.Soc.Lond.* A, **434**(1991)15-17).

[36] K. Gersten and H. Herwig, Stömungsmechanik Grundlagen der Impuls-,Wärme-und Stoffübertragung aus asymptotischer Sicht. Vieweg-Verlag, Braunschweig, Wiesbaden (1992).